Primary keratinocyte model of actinic keratosis reveals UV-induced DNA damage accumulation and persistent IFN signaling

Leonardo Elsbroek[1,2], Katja Reuschlein[1], Syrus Karsai[3,4], Anna Geueke[1], Mareike von Petersdorff-Campen[3], Martina Bresch[3], Volker Steinkraus[3], Peter Weisenseel[3], Peter Wolf[1], Marc Winnefeld[1], Frank Lyko[2] and Ludger Kolbe[1]

Journal of Investigative Dermatology (2025) ■, ■—■; doi:10.1016/j.jid.2025.11.018

Actinic keratosis (AK) is a precancerous, UV-induced skin lesion that can progress to cutaneous squamous cell carcinoma. Although UVR drives field cancerization and immunosuppression in the skin, keratinocyte-intrinsic responses to chronic, low-dose UV exposure have been insufficiently studied in AK. We established a patient-derived in vitro model using primary keratinocytes from AK lesions and age-matched, sun-exposed skin to investigate how repeated low-dose UV irradiation shapes keratinocyte stress responses. Integrating morphological profiling, cyclobutane pyrimidine dimer quantification, and bulk RNA sequencing, we observed morphological remodeling and accumulating DNA damage in AK keratinocytes despite activation of DNA repair and unfolded protein response pathways. Transcriptomic analyses revealed constitutive and UV-enhanced IFN signaling in AK cells, including upregulation of innate DNA sensing and ISGylation genes. Meta-analysis of 5 independent datasets validated IFN pathway activation as a conserved feature of AK, and IFNα exposure further sensitized AK keratinocytes to UV-induced cyclobutane pyrimidine dimer accumulation. Immunohistochemistry confirmed lesion-specific enrichment of ISG15 and UBE2L6 in AK epidermis, indicating spatially confined IFN pathway activation in vivo. Our model uncovers sustained IFN signaling and attenuated DNA damage repair as keratinocyte-intrinsic features of AK, suggesting that persistent IFN responses may modulate UV-induced damage responses and contribute to early photocarcinogenesis.

Keywords: Actinic keratosis, DNA damage, IFN signaling, Photocarcinogenesis, UV stress

INTRODUCTION

UVR is the primary environmental driver of skin carcinogenesis and a major contributor to field cancerization, a process in which chronically sun-exposed skin accumulates genetic mutations and epigenetic alterations. A hallmark of field cancerization is the development of actinic keratosis (AK), a precancerous lesion that can progress to cutaneous squamous cell carcinoma (cSCC) (Winge et al, 2023).

Early photocarcinogenesis is driven by mutations in tumor suppressor genes such as *TP53* and *NOTCH1/2*, which are already found in sun-exposed skin. The genomic landscape of skin cancer progression has been extensively investigated through integrative genomic mutation studies, which identified heterogeneous mutations in genes regulating apoptosis, epidermal differentiation, the cell cycle, and epigenetic remodeling (Kim et al, 2022; Li et al, 2015; Thomson et al, 2021). Furthermore, diseases associated with defective DNA damage response (DDR), for example, xeroderma pigmentosum and ataxia-telangiectasia, carry a high risk for skin cancer, underscoring the importance of intact DDR pathways (DiGiovanna and Kraemer, 2012; Dunn et al, 2006). Interestingly, ataxia telangiectasia mutated models highlighted the immunogenic crosstalk of the DDR through activation of IFN signaling (Sinha et al, 2025). Furthermore, increased AK and cSCC risk in immunocompromised patients underscores the importance of functional immune surveillance (Iannacone et al, 2016).

Additional evidence further highlights a critical interplay between the DDR and innate DNA-sensing pathways in keratinocytes (Dunphy et al, 2018). UV-induced DNA damage can act as a damage-associated molecular pattern for DNA sensors such as cGAS, IFI16, AIM2, and ZBP1 (Li et al, 2021; Skopelja-Gardner et al, 2020). These innate DNA sensors activate IFN signaling, NF-κB, and the NLRP3 inflammasome, leading to proinflammatory IFN and cytokine secretion and cellular senescence (Li et al, 2021; Yang et al, 2017). Acute activation of these pathways supports antigen

[1]Beiersdorf AG, Research and Development, Hamburg, Germany; [2]Division of Epigenetics, DKFZ-ZMBH Alliance, German Cancer Research Center, Heidelberg, Germany; [3]Dermatologikum Hamburg GmbH, Hamburg, Germany; and [4]Department of Dermatology and Venereology, University Medical Center Hamburg-Eppendorf, Hamburg, Germany

Correspondence: Leonardo Elsbroek, Beiersdorf AG, Research and Development, Beiersdorfstraße 1—9, Hamburg 22529, Germany. E-mail: l.elsbroek@web.de

Abbreviations: AK, actinic keratosis; CPD, cyclobutane pyrimidine dimer; cSCC, cutaneous squamous cell carcinoma; DDR, DNA damage response; DEG, differentially expressed gene; EdU, 5-ethynyl-2′-deoxyuridine; HEK, healthy epidermal keratinocyte; ISG, IFN-stimulated gene; SCC, squamous cell carcinoma; STAT, signal transducer and activator of transcription

Received 25 September 2025; revised 26 November 2025; accepted 29 November 2025; accepted manuscript published online XXX; corrected proof published online XXX

© 2025 The Authors. Published by Elsevier, Inc. on behalf of the Society for Investigative Dermatology.

presentation and immune-mediated clearance of damaged cells, whereas chronic activation can disrupt tissue homeostasis, compromise DDR, and foster a proinflammatory microenvironment (Li and Chen, 2018). Furthermore, UV studies of patients with lupus erythematosus highlighted UVB-responsive IFN genes as critical regulators to UVB photosensitivity, inflammation, and autoimmunity (He et al, 2025).

IFN-α pathways are known to play a tumor-suppressive role in the skin, and intralesional IFN-α injections (Edwards, 1992) or topical toll-like receptor 7 agonists, such as imiquimod, partially activate IFN pathways to promote AK regression (Torres et al, 2007). However, in a chronic inflammatory context, dysregulated IFN signaling may instead contribute to carcinogenesis, through the sustained expression of IFN-stimulated genes (ISGs) such as ISG15 and IFIT3. These ISGs have been shown to modulate the DDR, promote inflammation-driven tumor progression, and support the development of a tumor microenvironment (Kang et al, 2022; Wu et al, 2025) and were recently implicated in cSCC development (Zou et al, 2023).

It is crucial to investigate keratinocyte-intrinsic regulatory mechanisms triggered by repetitive low-dose UV exposure in AK because current knowledge is limited to studies in healthy keratinocytes (Dalmau et al, 2018; de Pedro et al, 2018) or mouse models (Lin et al, 2022) and remains poorly understood in AK. Especially low-dose UV induces cumulative DNA damage without overt inflammation or erythema (Young et al, 2007) and represents a key factor for AK and cSCC development (Traianou et al, 2012; Xiang et al, 2014).

To address this knowledge gap, we established an AK in vitro model by isolating primary keratinocytes from dermatologically excised AK lesions and comparing them with keratinocytes derived from age-matched, sun-exposed but nonlesional skin. Primary keratinocytes of both origins were subjected to single and repeated low-dose solar-simulated UV irradiation, which simulated chronic environmental UV stress. By integrating high-content morphological profiling, quantitative DNA damage assays, and transcriptomic analyses, we identified persistent activation of IFN signaling as a keratinocyte-intrinsic feature associated with DNA damage accumulation in primary keratinocytes from AK lesions.

RESULTS

Establishment of a primary in vitro model for AK

To characterize keratinocyte-intrinsic responses to UV-induced stress in AK, we developed a primary in vitro model using keratinocytes isolated from lesional skin biopsies of 16 clinically diagnosed patients with AK (Figure 1a and Table 1). Each experimental assay included multiple donors ($n = 4–10$) to ensure representative coverage and reduce the effects of interdonor variability. All samples originated from histologically confirmed AK fields. Cultured AK keratinocytes retained their basal epithelial morphology and expression of keratin 14, which was comparable with that of primary healthy epidermal keratinocytes (HEKs) and consistent with a basal keratinocyte phenotype (Figure 1b).

Targeted gene expression profiling through a tumor signaling panel revealed a distinct principal component analysis clustering of AK keratinocytes compared with that of HEK derived from both sun-exposed and non–sun-exposed skin (Figure 1c). Among the most differentially expressed genes (DEGs) were innate immune and IFN-related genes, including *CGAS*, *TLR3*, *IRF1*, and *CEACAM1*, indicating a proinflammatory and IFN-primed state (Figure 1d). Notably, AK keratinocytes exhibited partial transcriptomic overlap with the established cSCC cell line HSC1 (Kondo and Aso, 1981), suggesting distinct and potentially malignant changes in the transcriptional profile of AK keratinocytes.

Despite the limited scope of the tumor signaling panel, these data highlight consistent transcriptional divergence of isolated primary AK keratinocytes and support the feasibility and relevance for the primary AK in vitro model.

UV induces distinct morphologies in primary keratinocytes

For physiological in vitro UV exposure, AK and facial HEK cells were subjected to either a single or repetitive dose (3 consecutive days) of solar-simulated UV irradiation (relative 100 mJ/cm^2/day UVB) (Supplementary Figure S1), mimicking chronic low-dose solar exposure (Mann et al, 2020) (Figure 1e). Morphological changes were assessed through cell painting (Bray et al, 2016) with organelle- and structure-targeting dyes (Figure 2a) (Stirling et al, 2021). Compared with unirradiated keratinocytes, cell painting revealed pronounced morphological reorganization, including altered organelle structure and cytoskeletal rearrangement by Hoechst, MitoTracker, Concanavalin A, wheat germ agglutinin, and phalloidin staining (Figure 2a). Morphological profiling of cell features (Supplementary Figure S2a) revealed dose-dependent phenotypic remodeling visualized by Uniform Manifold Approximation and Projection clustering, with repetitive UV exposure inducing the most pronounced shift and distinct clustering. Crucially, Uniform Manifold Approximation and Projection clustering also diverged between AK and HEK cells, indicating basal morphological differences (Figure 2b). We then used a random forest model to deconvolute the most important features (Figure 2c and Supplementary Figure S2b). Top-ranked features included nuclear and cellular size as well as the structural granularity of mitochondria, endoplasmic reticulum, and actin–Golgi–plasma membrane compartments, highlighting both intrinsic and UV-induced morphological differences in AK cells. UV-induced damage to these organelles and their role in mediating UV stress are well-described in the endoplasmic reticulum (Bahamondes Lorca and Wu, 2023) and mitochondria (Yuan et al, 2025).

These phenotypic data suggest that the morphological changes after repetitive UV exposure reflect cumulative cellular damage and/or adaptive cellular remodeling in keratinocytes.

AK keratinocytes accumulate DNA damage after UV exposure

We next assessed whether morphological remodeling corresponds to cumulative DNA damage by measuring cyclobutane pyrimidine dimer (CPD) formation in keratinocyte nuclei through immunofluorescence (Figure 3a) and image-based analysis (Figure 3b). Six hours after irradiation, AK keratinocytes subjected to repeated UV stress exhibited higher CPD intensity than after a single UV exposure. Furthermore, CPD intensity levels were significantly elevated

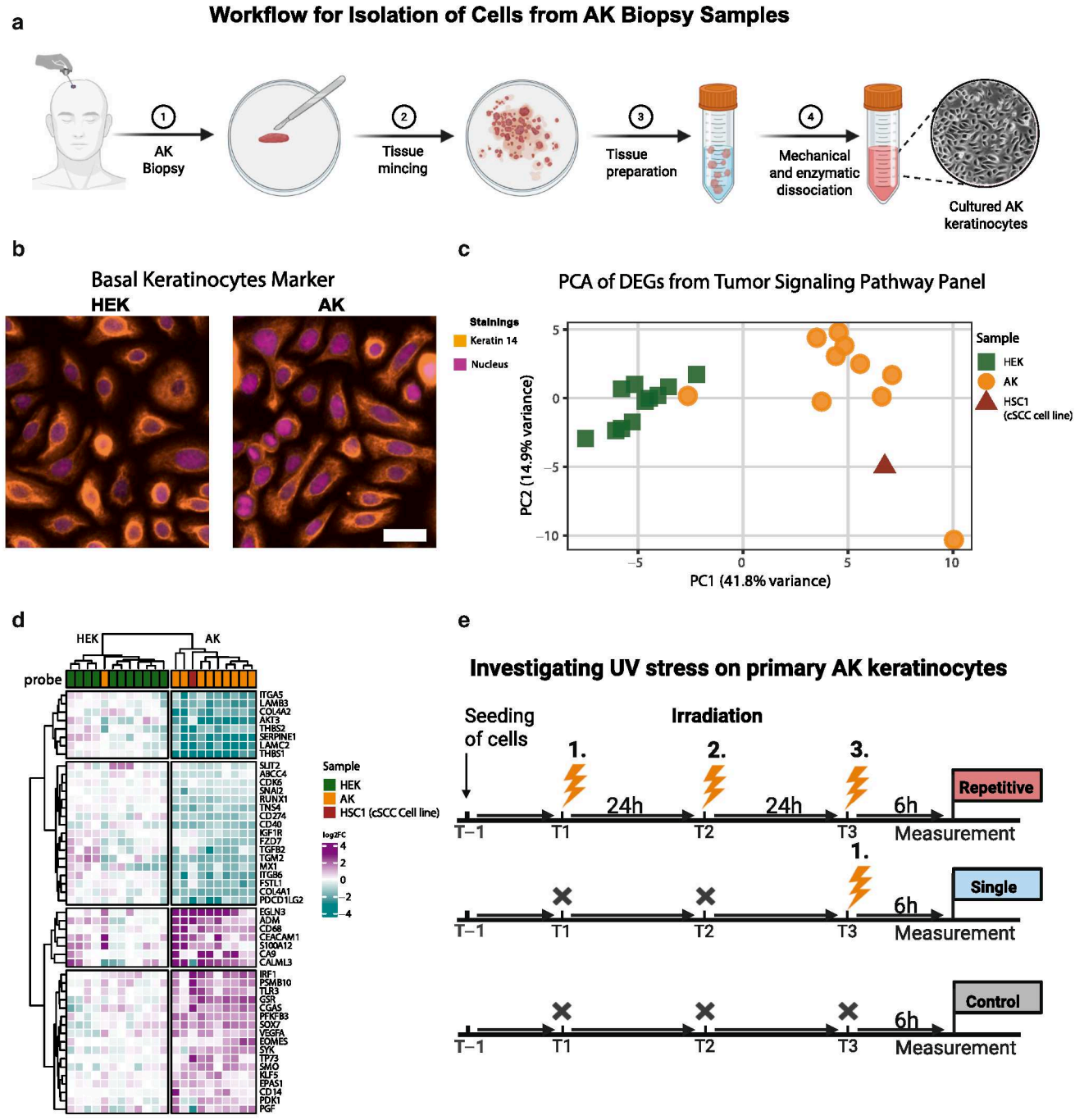


Figure 1. Primary keratinocytes derived from AK lesions retain basal identity and display distinct transcriptional profiles. (**a**) Schematic overview of the isolation and cultivation workflow for primary keratinocytes from AK shave biopsies. (**b**) Representative immunofluorescence staining of HEKs and AK keratinocytes at passage 3. Basal keratinocytes are labeled with K14 (orange); nuclei are counterstained with DRAQ5 (magenta). Bar = 25 μm. (**c**) PCA of transcriptomic profiles based on DEGs in tumor-related signaling pathways. HEK (n = 11), AK (n = 10), and cSCC cell line HSC1 (n = 1). (**d**) Heatmap of DEGs between HSC1, AK keratinocytes, and HEKs (adjusted $P < .01$; $\log_2FC \geq 0.5$). (**e**) Experimental design for investigating cellular responses to single and repetitive low-dose UV exposure in primary keratinocytes. AK, actinic keratosis; cSCC, cutaneous squamous cell carcinoma; DEG, differentially expressed gene; FC, fold change; HEK, healthy epidermal keratinocyte; K14, keratin 14; PC, principal component; PCA, principal component analysis.

compared with that of nonirradiated AK controls (adjusted $P = .006$) and HEK controls (adjusted $P = .007$), indicating DNA damage accumulation in AK cells (Figure 3c).

Twenty-four hours after irradiation, the CPD levels had decreased, indicating partial DNA repair. However, AK keratinocytes still retained significantly increased CPD intensity (Figure 3d), indicating slower DNA repair mechanisms than in HEK cells. Effect size analysis revealed consistent trends at both 6 and 24 hours, with stronger effects in AK (r = 0.58–0.62) than in HEK (r = 0.40–0.47) cells (Figure 3e and f). Although direct pairwise comparisons of irradiation did not reach adjusted significance (Supplementary Table S1),

Table 1. Clinical and Experimental Characteristics of Actinic Keratosis Donor Keratinocytes

Sample Description					Experiment					
Location	AKASI	Sex	Phototype	Age, y	RNA Sequencing	CPD	IFN	Ncounter	CP	EdU
Face	4.4	Female	2	88	✓		✓	✓		
Forehead	14	Female	2	81		✓	✓			
Forehead	8	Male	1	85				✓		
Forehead	7.4	Male	2	85				✓		
Forehead	6.2	Male	2	77				✓	✓	
Left side of the head	7.4	Male	1	84	✓		✓			
Nose	11.4	Male	2	70		✓	✓			
Occiput	6.6	Male	2	88	✓	✓			✓	
Occiput	6	Male	2	86				✓		
Occiput	5.8	Male	2	77	✓		✓	✓	✓	✓
Occiput	3.6	Male	2	85	✓	✓	✓		✓	✓
Scalp	7.6	Male	2	83			✓	✓	✓	
Scalp	7.1	Male	3	81	✓	✓		✓	✓	
Scalp	5.4	Male	2	83	✓	✓			✓	✓
Scalp	5	Male	2	82				✓	✓	✓
Scalp	4	Male	2	66			✓	✓		
16 Samples	6.8		2	81	7	6	8	10	8	4

Abbreviations: AK, actinic keratosis; AKASI, Actinic Keratosis Area and Severity Index; CP, cell painting; CPD, cyclobutane pyrimidine dimer; EdU, 5-ethynyl-2′-deoxyuridine.

Sixteen primary AK keratinocyte cultures were characterized by lesion location, gender, AKASI score, and donor age. Columns indicate the respective experiment: RNA sequencing, CPD immunostaining, IFN-α treatment, NanoString (nCounter), EdU proliferation, and CP assays. Check marks denote samples used in each assay. Multiple donors were included to ensure biological diversity and limit interdonor variability. Samples were excluded if cell yield was insufficient or stocks were depleted. Because AK samples were limited, the study design prioritized inclusion of diverse donors across assays rather than using every donor for all experiments.

groupwise graded effects further indicate progressive CPD accumulation upon repetitive irradiation and support impaired or delayed DNA repair in actinic keratinocytes.

To further distinguish proliferation-driven dilution from repair-mediated CPD reduction, we performed 5-ethynyl-2′-deoxyuridine (EdU) assays. Under identical culture conditions, AK keratinocytes and HEKs showed no basal difference in proliferation. Single and repetitive UV exposures reduced proliferation in both cell types, with a significant decrease in repetitively irradiated AK cells (adjusted $P < .05$) (Supplementary Figure S3a). Ranked effect sizes of UV-decreased proliferation indicated a larger effect in AK than in HEK (Supplementary Figure S3b). However, the overall UV-induced growth reduction was comparable between AK and HEK, indicating that CPD persistence in AK cells primarily reflects impaired DNA-repair kinetics rather than proliferation-driven dilution of unrepaired lesions after repetitive irradiation (Dorr and Rochette, 2023). Persistent DNA lesions increase mutagenic risk by spontaneous deamination of 5-methylcytosines and C→T transitions (Lee and Pfeifer, 2003).

Transcriptomic profiling reveals increased stress responses in HEKs and AK keratinocytes after repetitive UV stress

To dissect the underlying UV-induced mechanisms, we performed bulk RNA sequencing of untreated, single-dose, and repetitively UV-irradiated AK and HEKs 6 hours after single and repetitive irradiation. This analysis revealed distinct transcriptional programs, with principal component analysis showing separation by UV treatment independent of cell type, with repetitive exposure inducing the most defined cluster (Figure 4a). Independent of cell type, differential gene expression analysis revealed 4025 DEGs with repetitive UV irradiation and 2739 DEGs in the single-dose irradiation (adjusted $P < .05$, $\log_2$ fold change ≥ 0.5, chi-square $P < .001$) (Supplementary Figure S4a). Although DEG sets were overlapping, both treatments induced distinct gene sets, with a predominant trend toward down-regulation (Figure 4b). Subsequently, we performed comparative analysis across AK and HEK treatment groups, which revealed the greatest number of DEGs between UV-irradiated AK cells and untreated HEK controls (Supplementary Figure S4b).

Gene set enrichment analysis and gene set variation analysis across all treatment groups revealed a progressive upregulation of stress response pathways, including DNA repair, p53 signaling, oxidative phosphorylation, and the unfolded protein response, compared with that of unirradiated keratinocytes (Figure 4c and d). Gene set variation analysis further highlighted a dose-dependent increase in pathway activity with repetitive UV exposure (Figure 4d). Notably, the expression of key DDR effectors such as RRM2B, DDB2, POLH, and MDM2 increased progressively from single to repetitive irradiation (Figure 4a and Supplementary Figure S4f), indicating transcriptional adaptation to sustained UV stress. The overall robust UV induction of RRM2B, POLH, and XPC after UV exposure indicates that HEK and AK cells retain functional TP53 signaling (Figure 4d and e).

To explore the underlying mutations in our samples, we performed RNA-sequencing–based hotspot calling from clinically annotated variants, focusing on single nucleotide

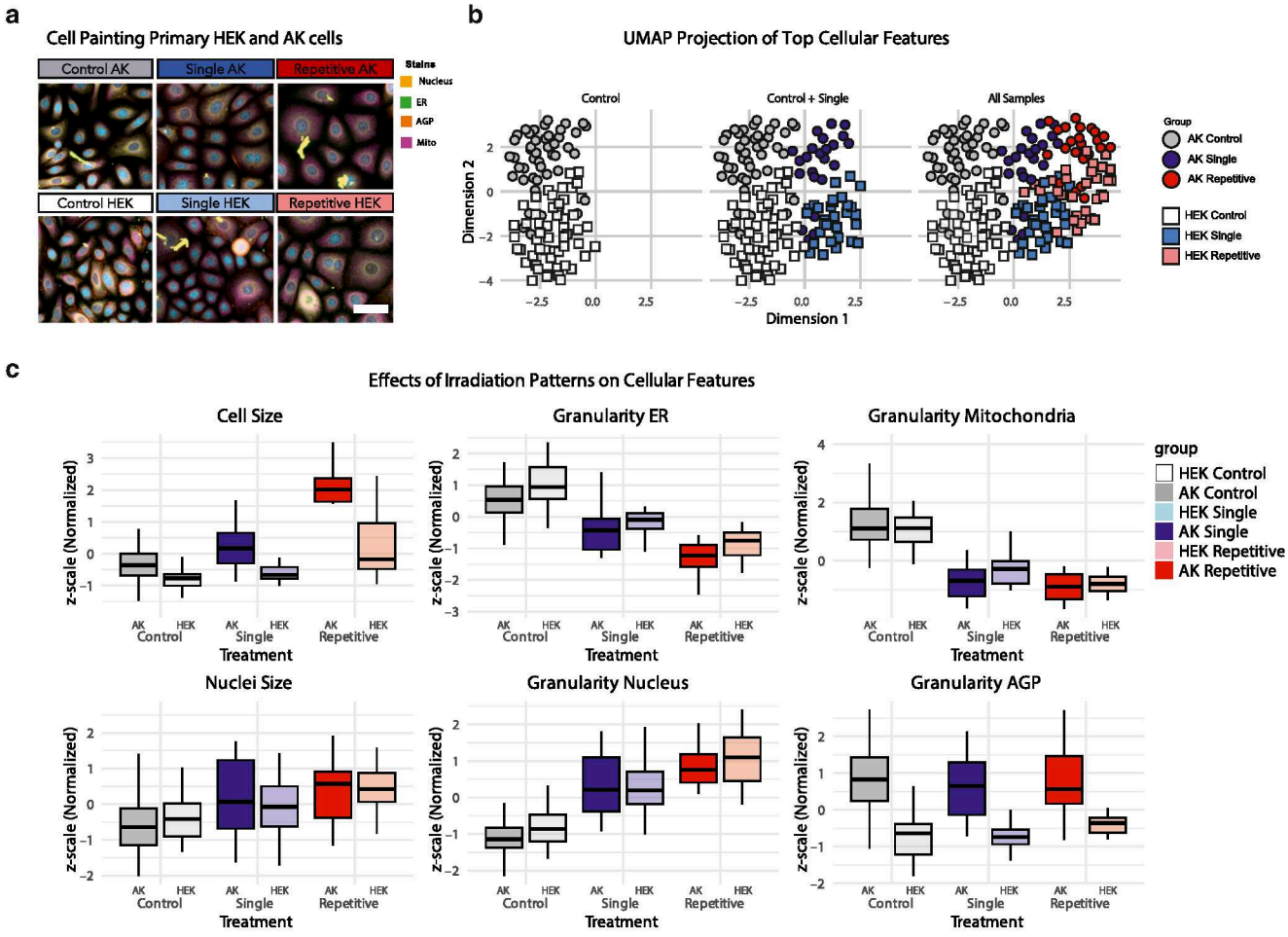


Figure 2. Morphological profiling reveals UV-induced and AK-intrinsic phenotypes. (**a**) Representative cell painting images of HEKs and AK keratinocytes under control conditions, single UV exposure, or repeated UV irradiation. Organelle-specific stains: nuclei (Hoechst, blue), ER (concanavalin A—Fluor 488, green), Golgi and plasma membrane (WGA—Fluor 555, orange), actin (phalloidin—Fluor 568, red orange), and mitochondria (Fluor 641, magenta). Bar = 50 μm. (**b**) UMAP projection of high-dimensional morphological features extracted from image-based profiling. Samples are colored by condition: HEK control (white squares), single-irradiated HEK (light blue), repeated-irradiated HEK (light red), AK control (dark gray circles), single-irradiated AK (dark blue), and repeated-irradiated AK (dark red). (**c**) Boxplots of selected morphological features identified by random forest classification. Features include nuclear size, cell size, ER granularity, mitochondrial granularity, nuclear granularity, and AGP granularity. Colors correspond to panel **b** (HEK: n = 8 donors, AK: n = 8 donors). AGP, actin—Golgi—plasma; AK, actinic keratosis; ER, endoplasmic reticulum; HEK, healthy epidermal keratinocyte; UMAP, Uniform Manifold Approximation and Projection; WGA, wheat germ agglutinin.

allele frequency of TP53 and other frequently mutated genes (Supplementary Figure S4g). The analysis showed that most cells expressed wild-type TP53 transcripts, with low-frequency TP53 mRNA variants (1—10% allele frequency), indicative of subclonal mutations in both AK and HEK samples (Supplementary Figure S4h). This pattern aligns with previous reports showing that even small regions of sun-exposed skin (≈1 mm^2) can harbor complex clonal architectures of *TP53* and *NOTCH1* variants (Martincorena et al, 2015). A full characterization of the mutational landscape in primary cells will require targeted or whole-exome sequencing of clonally expanded AK keratinocytes.

Together, these findings suggest increased activation of repair mechanisms in response to repetitive UV exposure. Furthermore, the results indicate that transcriptional activation of repair machinery alone is insufficient to prevent accumulating DNA damage, especially in actinic keratinocytes.

AK keratinocytes exhibit sustained IFN signaling and inflammasome activation

Next, we further elucidated the mechanisms contributing to the increased UV sensitivity in AK keratinocytes by focusing on the comparison between AK and HEK. Gene set variation analysis revealed robust and consistent upregulation of IFN-α and γ signaling pathways in AK cells, both under basal conditions and after UV exposure (Figure 4c—e and Supplementary Figure S4d). Key markers of IFN pathways, for example, signal transducer and activator of transcription (STAT) 2 and ISG15, were significantly regulated (Figure 4f and g and Supplementary Figure S4e).

The nuclear damage-associated molecular pattern sensor IFI16, which links nuclear DNA sensing to IFN activation, was significantly upregulated in AK keratinocytes after UV irradiation. Importantly, IFI16 and cGAS mediate the expression of proinflammatory cytokines IL-1B and IL-18, which were also upregulated in AK cells (Figure 4f),

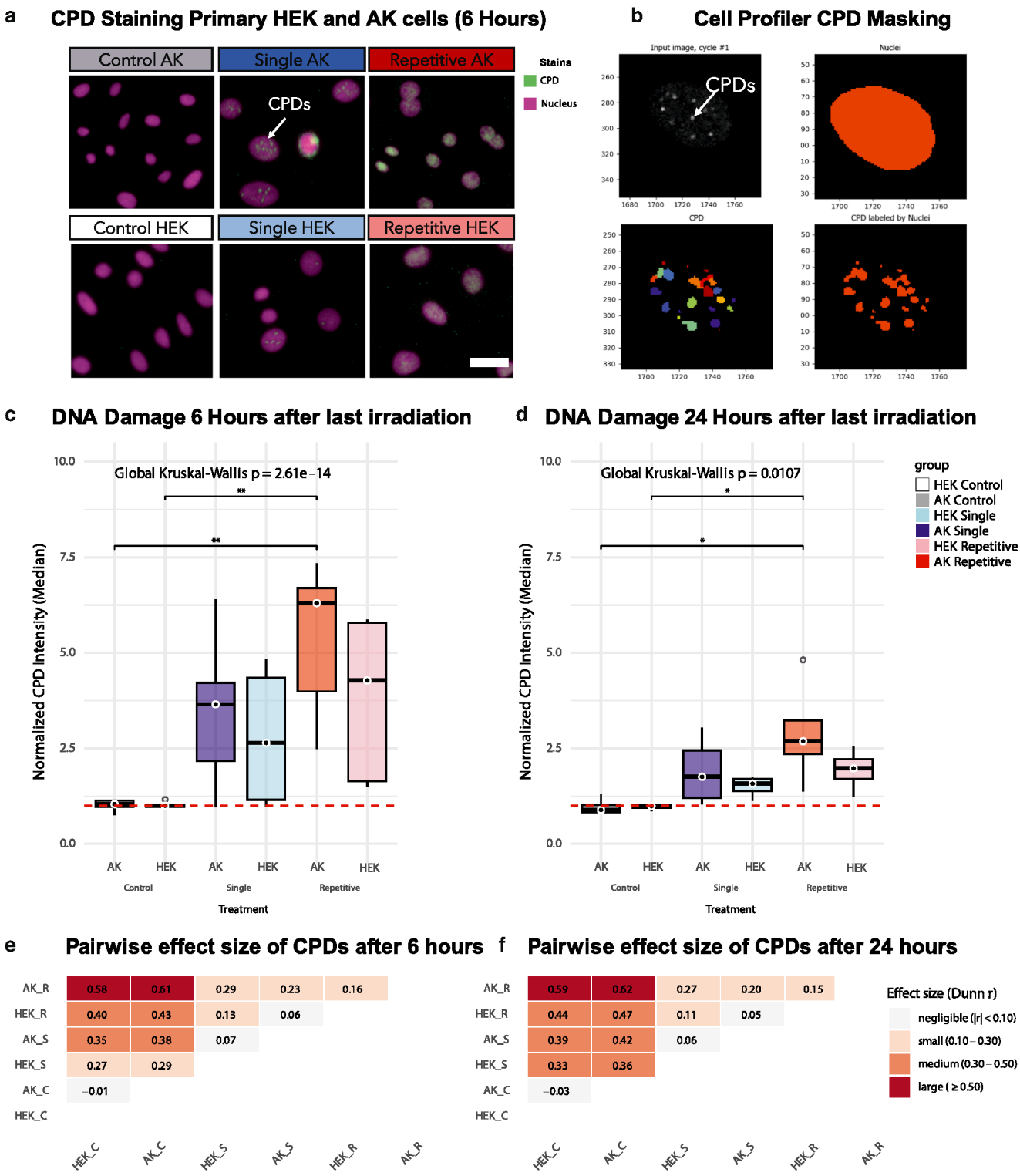


Figure 3. Actinic keratinocytes accumulate UV-induced DNA damage after repetitive exposure. (**a**) Representative immunofluorescence images of CPD staining (green) and DRAQ5 nuclear counterstaining (magenta) in HEKs and AK keratinocytes under different UV treatment conditions. Bar = 30 μm. (**b**) Masked images used to quantify CPD foci through CellProfiler. (**c**) Median-normalized CPD intensity 6 hours after irradiation. CPD levels were normalized to unirradiated HEK controls; the red dashed line denotes baseline. Statistical significance was first evaluated using the Kruskal–Wallis test, followed by Dunn's posthoc test for pairwise group comparisons (HEK: n = 5 donors, AK: n = 6 donors). (**d**) Median-normalized CPD intensity 24 hours after irradiation. Color coding: HEK control (white), single UV (light blue), repeated UV (light red), AK control (dark gray), single UV (dark blue), and repeated UV (dark red). (HEK: n = 4 donors, AK: n = 4 donors). (**e, f**) Heatmap of ranked pairwise effect size from Dunn's posthoc test of CPDs after 6 and 24 hours. The color scale represents the magnitude and direction of the effect size, binned as small ($r < 0.3$), medium ($0.3 \leq r < 0.5$), and large ($r \geq 0.5$). AK, actinic keratosis; CPD, cyclobutane pyrimidine dimer; HEK, healthy epidermal keratinocyte.

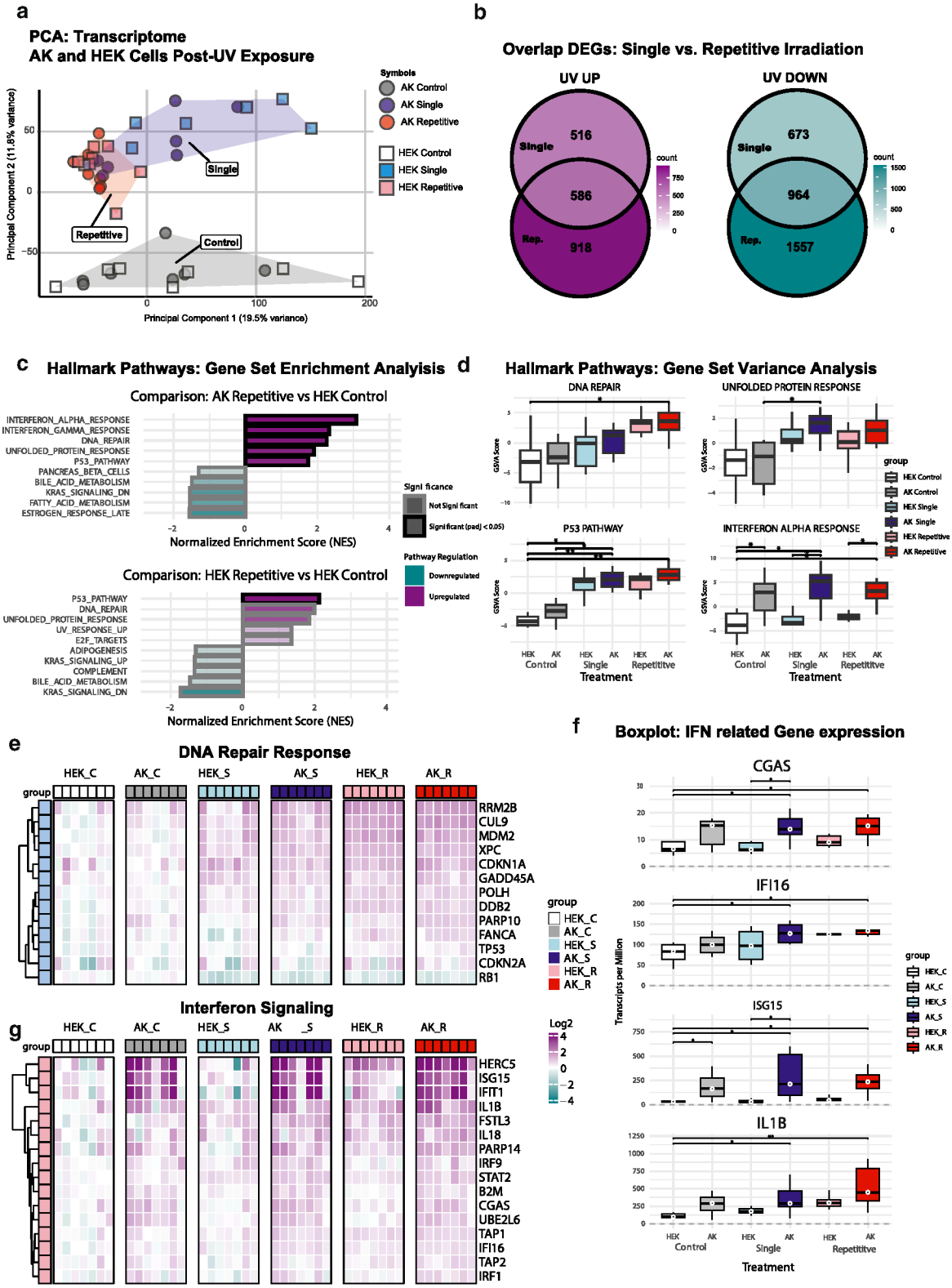


Figure 4. Transcriptomic profiling reveals distinct UV stress responses and dysregulated IFN signaling in AK keratinocytes. (**a**) PCA of global transcriptomic data from HEKs and AK keratinocytes under control, single, and repetitive UV treatment (n = 7 per group). Samples are colored by condition: HEK control (white squares), single-irradiated HEK (light blue), repeated-irradiated HEK (light red), AK control (dark gray circles), single-irradiated AK (dark blue), and repeated-irradiated AK (dark red). (**b**) Venn diagrams showing overlap of upregulated (magenta) and downregulated (turquoise) DEGs between UV conditions. DEGs: adjusted $P < .05$, $\log_2 FC \geq 0.5$. (**c**) GSEA of Hallmark gene sets for repetitively irradiated AK and HEK cells versus HEK control. Significant pathways (FDR < 0.05) are outlined in black. (**d**) GSVA boxplots for Hallmarks gene sets of DNA repair, UPR, p53, and IFN-α response. Statistical analysis by Kruskal–Wallis with Dunn's posthoc test. (**e**) Heatmap with significantly DEGs from pathways associated with DNA repair color scaling indicates $\log_2$ FCs. (**f**) Boxplots for CGAS, IFI16, IL1B, and ISG15. Statistical analysis by Kruskal–Wallis with Dunn's posthoc test. (**g**) Heatmap with significantly DEGs from pathways associated with IFN signaling. Scaling is as in **e**. AK, actinic keratosis; DEG, differentially expressed gene; FC, fold change; FDR, false discovery rate; GSEA, gene set enrichment analysis; GSVA, gene set variation analysis; HEK, healthy epidermal keratinocyte; PCA, principal component analysis; UPR, unfolded protein response.

indicating inflammasome engagement in AK under chronic UV exposure. The ubiquitin-like modifier ISG15, a key effector of IFN signaling involved in DNA damage tolerance and p53 regulation (Sandy et al, 2020), showed the most pronounced differential expression among ISGs (Figure 4e and f), with significantly elevated levels across all AK conditions independent of UV. Accordingly, genes of the ISGylation machinery, *UBE2L6* and *HERC5*, were also significantly upregulated, suggesting enhanced ISGylation activity in AK keratinocytes (Figure 4f and g and Supplementary Figure S4e). Furthermore, AK keratinocytes presented increased expression of IFN-mediated antigen processing and presentation genes, including *TAP1*, *TAP2*, *B2M*, and *IRF1*, indicating increased immunogenicity through IFN signaling in AK keratinocytes (Figure 4g).

These findings highlight persistent IFN signaling as a defining feature of AK keratinocytes, potentially contributing to UV hypersensitivity and inflammasome activation. Furthermore, increased expression of IFI16, STAT2, and IL-1B after single and repetitive UV exposure suggests a possible priming of IFN and inflammasome responses in AK keratinocytes.

Meta-analysis and single-cell profiling support IFN signaling as a shared feature of AK lesions and squamous cell carcinoma–associated keratinocytes

We then further validated our transcriptomic findings with in vivo samples by integration of 5 independent transcriptomic datasets of AK lesions to perform a meta-analysis (GSE2503, GSE98774, GSE42677, GSE84293, and GSE90643) (Figure 5a). Hallmark and Reactome pathway analyses consistently identified IFN signaling as a significantly enriched pathway across datasets (Figure 5b and Supplementary Figure S5a). To further investigate the role of IFN signaling in the progression of AK, we analyzed single-cell transcriptomic data from squamous cell carcinoma (SCC)–associated keratinocytes (Zou et al, 2023). Pathway analysis of this SCC-specific keratinocyte subpopulation revealed activation of the IFN response (Figure 5d). Notably, *ISG15*-positive cells strongly coexpressed CDKN2A, a key regulator of cellular senescence and tumor suppression (Supplementary Figure S5c) (Kim et al, 2022). The expression of ISG15, UBE2L6, and STAT2 in the SCC subpopulation further supported a role in SCC pathogenesis (Supplementary Figure S5c and d).

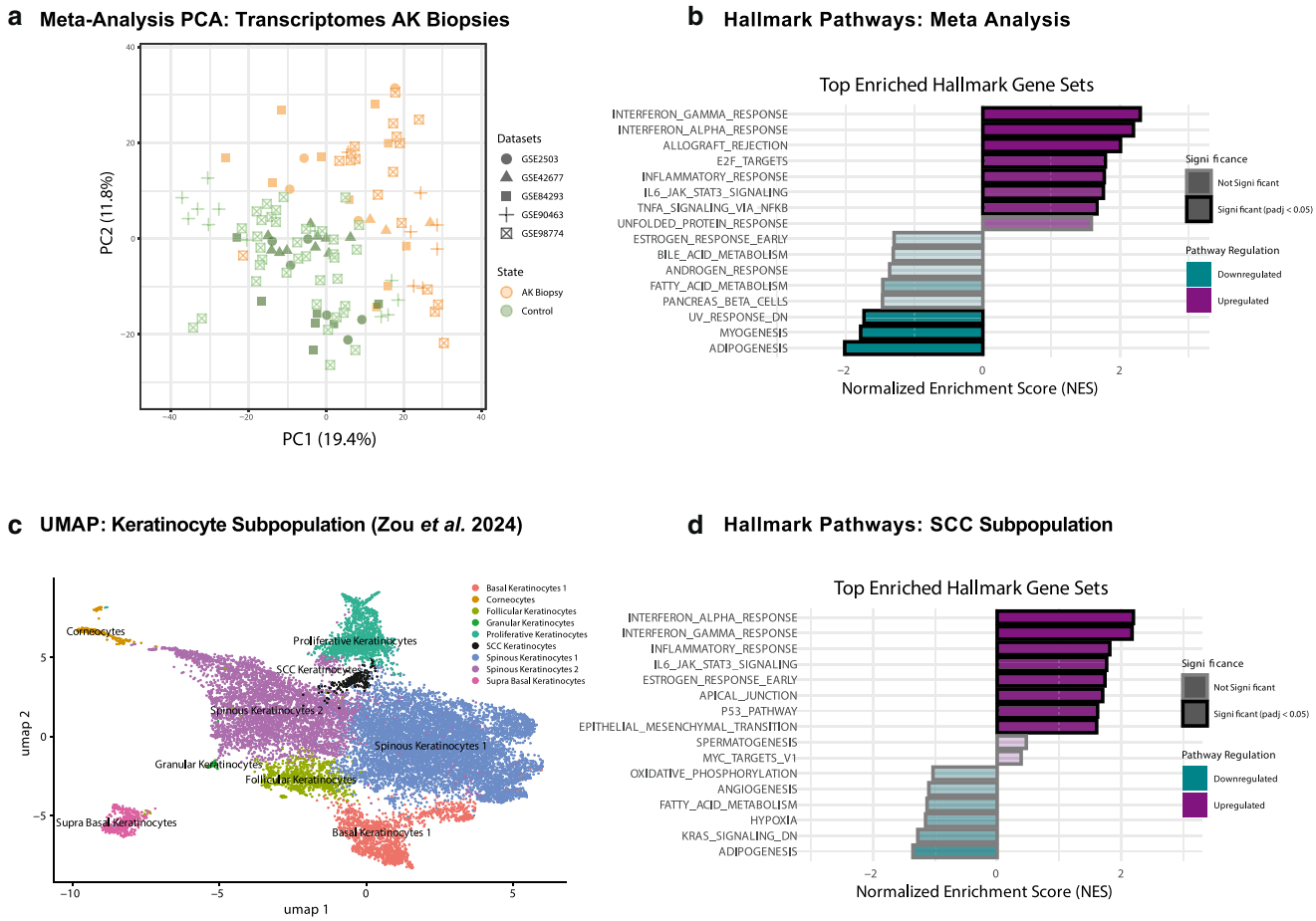


Figure 5. Meta-analysis confirms IFN signaling as a hallmark of AK and SCC progenitor keratinocytes. (**a**) PCA of 5 AK biopsy datasets (GSE2503, GSE42677, GSE84293, GSE90643, and GSE98774) with batch correction. Color = group, shape = dataset. (**b**) Hallmark pathway analysis of 5 AK biopsy datasets. Upregulated (magenta) and downregulated (turquoise) pathways are shown as $\log_2$ fold changes; adjusted *P*-value significance is outlined in black. (**c**) UMAP projection of keratinocyte subpopulations from Zou et al (2023) scRNA-seq data. SCC-associated cluster is highlighted in black. (**d**) Hallmark Pathway Analysis of SCC progenitor cluster. Upregulated (magenta) and downregulated (turquoise) pathways are shown; significance is outlined in black. AK, actinic keratosis; PCA, principal component analysis; SCC, squamous cell carcinoma; scRNA-seq, single-cell RNA sequencing.

These findings indicate a link between IFN activation and early SCC transformation, highlighting sustained IFN signaling as a defining characteristic of epithelial carcinogenesis emerging from AK.

ISG15 and UBE2L6 are markers for AK lesions

Immunohistochemical analysis of actinic, perilesional, and healthy facial skin revealed distinct patterns of the IFN-associated markers ISG15 and UBE2L6 (Figure 6a). ISG15 staining was constrained within lesional epidermal areas, whereas perilesional and unaffected facial skin remained negative. Interestingly, within AK lesions, ISG15 expression was predominantly localized to the lower epidermal as well as dermal areas, indicating inflammatory crosstalk, whereas parakeratotic regions lacked detectable staining. Similarly, UBE2L6 expression was markedly upregulated in AK lesions compared with that in nonlesional and healthy tissue. Although overall staining intensity was higher in lesional areas, weak UBE2L6 staining was also observed throughout the epidermis of healthy controls, consistent with a basal level of expression in normal skin. These findings highlight ISG15 and UBE2L6 as markers of lesional AK keratinocytes and suggest their involvement in IFN-driven stress responses during early carcinogenic processes.

IFN-α enhances UV-induced DNA damage accumulation in AK keratinocytes

To examine the potential influence of IFN-α signaling on DNA damage accumulation, AK keratinocytes and HEKs were exposed to low-dose IFN-α (40 U/ml) after each round of repetitive UV irradiation (Figure 6b). AK keratinocytes exposed to repetitive UV irradiation exhibited higher CPD levels than HEK cells, consistent with impaired DNA damage resolution. Notably, IFN-α treatment further increased CPD accumulation specifically in AK keratinocytes, whereas HEK cells remained unaffected (Figure 6c). Pairwise permutation tests and rank-biserial effect sizes indicated large UV-induced increases in CPDs across groups. Importantly, the UV + IFN comparison showed that IFN-α–treated AK keratinocytes accumulated significantly more CPDs than HEK cells under identical conditions ($r = 0.78$, adjusted $P = .046$) (Supplementary Table S2). This indicates that IFN-α adds a further large, AK-specific increase in CPD accumulation. These findings establish a functional link between sustained IFN activation and impaired DNA repair, implicating persistent IFN signaling as a key contributor to UV hypersensitivity in AK.

Together, our results demonstrate that increased IFN signaling sensitizes AK keratinocytes to UV stress, amplifies UV-induced DNA damage accumulation, and promotes transcriptional inflammasome activation. Furthermore, in vivo AK lesions show increased ISG15 and UBE2L6 marker staining, and the observed expansion of IFN-activated keratinocyte subpopulations in SCC further supports a promoting role for sustained IFN signaling in early photocarcinogenesis.

DISCUSSION

Chronic UV stress drives AK and cSCC through mutations and epigenetic alterations (Brash et al, 1991; Solé-Boldo et al, 2022). Yet, how actinic keratinocytes differ from sun-exposed healthy keratinocytes in their UV response remains poorly understood. We exposed patient-derived AK keratinocytes to UV and identified persistent IFN signaling as a link to UV hypersensitivity, impaired DNA repair, and stress-induced transcriptional remodeling.

Profiling of UV stress response in AK keratinocytes revealed progressive changes and CPD accumulation despite induction of DNA-repair and TP53 pathways. RNA profiling showed similar subclonal TP53 mutations in HEK and AK cells, consistent with TP53 mosaicism in sun-exposed keratinocytes (Martincorena et al, 2015; Tandukar et al, 2024), indicating that TP53 status and activity alone are unlikely to explain UV hypersensitivity of AK keratinocytes.

Instead, transcriptional analysis of AK keratinocytes showed elevated basal and UV-induced IFN signaling. AK keratinocytes expressed increased levels of ISG15 and ISGylation enzymes (HERC5, UBE2L6), which were shown to regulate DNA translesion synthesis (Park et al, 2014) and to intensify DNA damage by replication fork acceleration (Raso et al, 2020). Furthermore, UV-induced IFI16, STAT2, IL-1B, and IL-18 indicated activation of the cGAS–STING axis (Almine et al, 2017), which can promote inflammation, senescence, and tissue injury (Chen et al, 2018; Feldmeyer et al, 2007). Consistent with this notion, dysregulated IFN signaling was linked to UV hypersensitivity in cutaneous lupus erythematosus (He et al, 2025). Functionally, IFN-α priming enhanced UV-induced CPD accumulation in AK keratinocytes but not in HEKs, indicating sensitization rather than sufficiency. IFN-α sensitization effects were reported for UVB-induced apoptosis in N/TERT keratinocytes (Loftus et al, 2024). Furthermore, prolonged IFN exposure can induce a transcriptional memory (Kamada et al, 2018), which contributes to immune dysfunction in cancer cells (Qiu et al, 2023), and the IFN-related DNA damage resistance signature has been suggested to remodel genotoxic stress responses (Weichselbaum et al, 2008). Thus, a persistent IFN signaling indicates that AK keratinocytes are likely in an IFN inflammatory state, which may contribute to UV hypersensitivity. Our immunohistology stainings further demonstrated strong ISG15 and UBE2L6 expression confined to actinic epidermis, and single-cell RNA sequencing revealed expansion of ISG15-positive keratinocytes in cSCC (Zou et al, 2023), indicating continuity from AK to cSCC (Rodríguez-Paredes et al, 2018). Furthermore, in vitro SCC models identified IFN-driven STAT1 as factor for invasion (Kumagai et al, 2022), and a recent meta study revealed that IFN signaling increases from AK to cSCC (Bencomo and Lee, 2024). Thus, our analysis indicates that IFN activation emerges as a defining molecular hallmark feature of AK, which is relevant for progression toward cSCC.

We hypothesize that persistent IFN signaling in actinic keratinocytes interferes with the UV stress response. Specifically, chronic activation of ISG15 and ISGylation enzymes (UBE2L6, HERC5) and nuclear DNA sensors (IFI16, cGAS) may alter DNA repair by modifying key DDR proteins and sustain inflammatory signaling. Aberrant IFN–DDR crosstalk could reduce CPD repair, promote CPD accumulation, and amplify UV-driven inflammatory responses, thereby supporting persistence and expansion of premalignant keratinocyte clones.

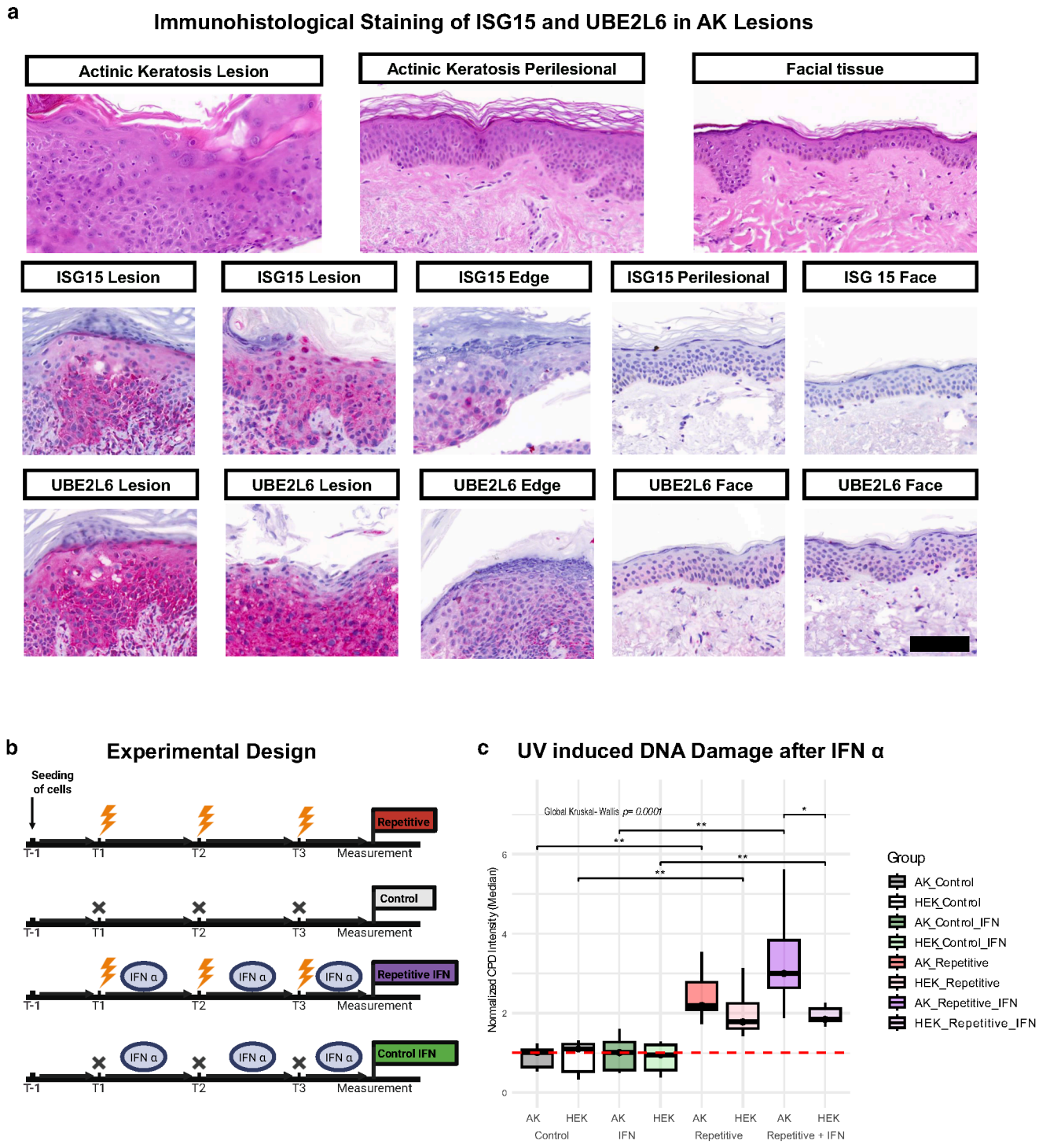


Figure 6. ISG15 and UBE2L6 mark lesional AK keratinocytes, and IFN-α activation is associated with increased UV-induced DNA damage. (**a**) Representative immunohistochemistry images of IFN markers *ISG15* and *UBE2L6* in AK lesions and sun-exposed facial control skin. AK samples show strong keratinocyte staining of lesional AK areas of lower epidermis with a gradual decline toward lesional edges and minimal signal in perilesional and control skin. Top row: H&E staining, second row: ISG15, third row: UBE2L6. Marker sections were counterstained with hematoxylin and developed using permanent red chromogen. Bar = 100 μm. (**b**) Experimental design of repetitive UV irradiation with IFN-α. (**c**) Median-normalized CPD intensity measured 6 hours after irradiation. CPD levels were normalized to unirradiated HEK controls (red dashed line indicates baseline). Statistical significance was assessed using the Kruskal–Wallis test, followed by pairwise permutation testing (HEK: n = 8 donors; AK: n = 9 donors). AK, actinic keratosis; CPD, cyclobutane pyrimidine dimer; HEK, healthy epidermal keratinocyte.

Limitations and future directions

Our AK model isolates keratinocyte-intrinsic IFN mechanisms but lacks immune components, representing a key limitation. In vivo, IFN-α is produced by plasmacytoid dendritic cells during skin injury, inflammation, and imiquimod treatment (Ueyama et al, 2014), which promotes immune

clearance of damaged lesional keratinocytes (Gregorio et al, 2010). Furthermore, plasmacytoid dendritic cell populations accumulate in cSCC (Bluth et al, 2009) and can be suppressed by UV-induced T-regulatory cell expansions (Shime et al, 2025). Immunosuppressed patients with cSCC exhibit diminished IFN signatures (Wenzel et al, 2008), highlighting the role of IFNs in tumor immunosurveillance of UV-exposed skin. Coculture experiments with immune cells will be necessary for dissecting epithelial–immune crosstalk under UV stress. A further limitation is the subclonal heterogeneity of the skin. Addressing this requires single-cell clonal expansion and DNA-based genotyping to define how clonal backgrounds influence UV stress responses. Future studies are needed to address how IFN signaling becomes persistent in actinic keratinocytes, how it modulates DNA-repair efficiency, and how epithelial IFN states shape immune surveillance. This is clinically relevant because IFN pathways contribute to immune clearance of malignant cells (Garcia-Diaz et al, 2017; Yu et al, 2022; Zeng et al, 2021). IFN-inducing therapy with imiquimod promotes AK regression (Ooi et al, 2006) but increases UV sensitivity (Lacarrubba et al, 2008), reinforcing the need for strict photoprotection in IFN-inflamed skin. Exploring IFN mechanisms and UV may ultimately help preventive and therapeutic strategies for UV-induced skin disease.

Our study establishes a primary patient-derived in vitro AK model and identifies persistent IFN signaling as a hallmark of UV hypersensitivity and impaired DNA repair in AK keratinocytes. The model provides a platform for dissecting epithelial stress responses and supports targeting IFN pathways to prevent progression from AK to cSCC.

MATERIALS AND METHODS

Isolation and cultivation of primary keratinocytes

AK shave biopsies were obtained with informed consent. For each investigated skin lesion, a representative biopsy was obtained confirming the diagnosis of AK. Samples were disinfected, trimmed, and digested overnight at 4 °C in DMEM (11885084, Gibco) with collagenase (200 U/ml) and Dispase (2 U/ml). After PBS washes, tissues were trypsinized (37 °C, 10–15 minutes), filtered (70 μm), and centrifuged (1200 r.p.m., 5 minutes). Cells were resuspended in DermaCult Keratinocyte medium (100-0500, Stem Cell Technologies) and seeded on collagen-coated plates. Nonadherent cells were removed after 24 hours. Cultures reached confluence in 3–5 days and were used up to passage 3. Isolation and culturing of control keratinocytes from sun-exposed facial skin were performed as previously described (Mann et al, 2020). Isolates were expanded for assays, and each experiment had a robust representation of donors to reduce potential interdonor variability. AK samples were collected over a 4-year period, and exclusions were based on sample availability. All experiments were conducted with identical seeding densities (5×10^4 cells/ml). AK and healthy keratinocytes exhibited comparable growth kinetics under identical culture conditions. Basal Keratinocyte marker staining was performed with anticytokeratin 14 antibody (SP53) (ab119695, Abcam, 1:500). IFN stimulation was induced with recombinant human IFN alpha 1 protein (ab48750, Abcam).

Irradiation and UV dosimetry

UV irradiation was performed using a 1600 W Oriel solar UV simulator (Newport, MA) equipped with a dichroic mirror (280–400 nm) and a N-WG320 long-pass filter (Schott, Germany) to reproduce the solar UV spectrum (Supplementary Figure S1). Prior to each experiment, UVB intensity was measured with an IL1700 Research Radiometer (Newport) equipped with an SED240 detector and A415 detector multiplexer. The detector was positioned at the level of the cell monolayer to measure the irradiance (W/m^2) of the Oriel solar simulator used for exposure. Irradiation was recorded at multiple positions across the exposure area to ensure homogeneity. Exposure time was adjusted to deliver a UVB dose of 100 mJ/cm^2 (dose = irradiance × time), which under our lamp settings corresponded to ~5 minutes of exposure. This dose is equivalent to 8 minutes of natural clear-sky midday summer daylight UV in northern Germany (Mann et al, 2020). To prevent photosensitization, media were replaced with PBS (with low calcium ion/magnesium ion) during exposure. For repetitive exposure, cells received daily doses for 3 consecutive days. Control wells were kept in PBS under identical conditions without UV exposure.

Cell painting assay

Cell painting was performed on the basis of the protocol by Bray et al (2016) using the PhenoVue Cell Painting Kit (PING11, Revvity) according to the manufacturer's instructions. Morphological staining was performed with Hoechst 33342 Nuclear Stain, Fluor 488 Concanavalin A, Fluor 555 wheat germ agglutinin, Fluor 568 Phalloidin, and 641 Mitochondrial Stain. Stains were applied to visualize nuclei, endoplasmic reticulum, plasma membrane/Golgi, actin cytoskeleton, and mitochondria, respectively. Images were acquired with the ImageXpress Pico Automated Cell Imaging System (Molecular Devices) using a ×20 objective and analyzed with CellProfiler 4.2.8 (Stirling et al, 2021). Morphological profiling and feature extraction were performed in R (version 4.3.3) using cytominer (0.2.2), ranger (0.17.0), and Uniform Manifold Approximation and Projection (0.2.10), with low-variance and highly correlated features removed prior to model training (Wright and Ziegler, 2017).

CPD DNA damage assay

CPDs were detected using the OxiSelect Cellular UV-Induced DNA Damage Staining Kit (CPD) (STA-327, Cell Biolabs) and stained according to the manufacturer's instructions. Nuclei were counterstained with DRAQ5 (62251, Thermo Fisher Scientific). Images were acquired using the Molecular Devices PICO Imaging System at ×20 magnification. Quantification of CPD signal was performed in CellProfiler 4.2.8 using speckle counting to measure nuclear CPD intensity and foci number per nucleus. All biological replicates were analyzed in technical triplicates with 9 images per well. Median nuclear CPD fluorescence intensity per nucleus was quantified and normalized to the HEK control.

EdU cell proliferation assay

Cell proliferation was analyzed using the Click-iT EdU Cell Proliferation Kit for Imaging, Alexa Fluor 488 (C10337, Invitrogen). Cells were incubated with 10 μM EdU for 2 hours, fixed for 15 minutes with 4% formaldehyde, and subsequently permeabilized in 0.5% Triton X-100 (Merck) in PBS for 20 minutes. Incorporated EdU was visualized through click chemistry with Alexa Fluor 488 azide, nuclei were counterstained with Hoechst 33342, and imaging was performed on the Molecular Devices PICO system (×20), and median EdU nuclei intensity was quantified using CellProfiler (Stirling et al, 2021).

Immunohistochemistry

AK and matched facial tissue samples were initially embedded in optimum cutting temperature compound and stored at −80 °C to preserve tissue integrity. For immunohistochemistry, tissues were fixed in formaldehyde, re-embedded in paraffin, and sectioned. Staining was performed on the Dako Omnis platform (Agilent). Sections were baked at 80 °C for 45 minutes, deparaffinized with Clearify (Agilent), and subjected to heat-induced epitope retrieval in Target Retrieval Solution (EDTA, pH 9; Agilent) for 18 minutes at 95 °C. After washing, sections were incubated for 20 minutes with primary antibodies diluted in Agilent Antibody Diluent: anti-ISG15 (mouse monoclonal, clone F-9, sc-166755, Santa Cruz Biotechnology; 1:40) and anti-UBE2L6 (rabbit monoclonal, clone 6H8L5, 703136, Invitrogen; 1:75). After washing, a biotinylated secondary antibody was applied for 15 minutes, followed by streptavidin–alkaline phosphatase (Agilent) for 15 minutes. Staining was visualized using the Permanent Red chromogen system (K0640, Agilent), counterstained with hematoxylin, dehydrated, and coverslipped.

RNA sequencing and transcriptomic analysis

Total RNA was extracted using RNeasy Mini kits (Qiagen, 74104), and library preparation and sequencing were performed by Novogene GmbH. Raw read counts were analyzed using DESeq2 (Love et al, 2014), with unirradiated HEKs serving as the reference group. Differential gene expression was defined as an adjusted $P < .05$ and an absolute $\log_2$ fold change ≥ 0.5. Gene set enrichment analysis (version 4.4.0) (Subramanian et al, 2005) and gene set variation analysis (version 1.50.5) (Hänzelmann et al, 2013) were performed using $\log_2$ fold changes and adjusted $P < .05$ with MSigDB Hallmark (Liberzon et al, 2015) and Reactome (Jassal et al, 2020) pathway databases. For meta-analysis, the following Gene Expression Omnibus datasets were included: GSE2503 (Nindl et al, 2006), GSE98774, GSE42677 (Mitsui et al, 2014), GSE84293 (Chitsazzadeh et al, 2016), and GSE90643 (Joly et al, 2018). Cross-dataset normalization, batch correction (ComBat), and comparative analyses were conducted using ExpressAnalyst (Ewald et al, 2023).

RNA variant calling

RNA-sequencing BAM files were analyzed for expressed single-nucleotide variants in *TP53*, *NOTCH1/2*, *CDKN2A*, *FAT1*, and *KMT2C*. Target loci were derived from ClinVar (Landrum et al, 2020), with gene intervals defined by GenomicFeatures (Lawrence et al, 2013) and aligned to the human genome assembly GRCh38.p14 (Schneider et al, 2017). Pileups were generated with Rsamtools (2.26.0) (base Q $\geq$ 20, MAPQ $\geq$ 20, max depth 2000) and annotated with VariantAnnotation (3.22), (Obenchain et al, 2014). Variants were detected if supported by $\geq$20× coverage, $\geq$5 ALT reads, nonreference background $\leq$20%, and a binomial false-discovery rate of $q < 1 \times 10^{-4}$. For visualization, thresholds (allele frequency $\geq$ 1%, coverage $\geq$ 50×) were applied to investigate subclonal variation. Maximum allele frequency was plotted as a heatmap for each sample, and lollipop plots were plotted for all observed *TP53* and *NOTCH1* alterations.

Single-cell RNA-sequencing analysis

Public single-cell RNA-sequencing data (Zou et al, 2023) (GSE193304) were processed with Harmony (Korsunsky et al, 2019) for batch correction and analyzed in Seurat (5.2.1) (Stuart et al, 2019). Clusters were annotated on the basis of the marker genes from the original publication.

Illustrations and figures

Schematic figures were created with BioRender (https://BioRender.com, Academic License, Elsbroek 2025). Data and statistical graphics were generated with ggplot2 (4.0.0).

Statistical analysis

All analyses were performed in R (version 4.3.3). Group comparisons were conducted using Kruskal–Wallis tests with Dunn's post-hoc and Benjamini–Hochberg correction. Effect sizes were calculated as rank-biserial correlations (r), derived from the standardized z statistic ($r = z / \sqrt{n}$), to quantify the magnitude of group differences in Dunn's tests. For the multifactorial UV + IFN experiment, pairwise permutation tests (10,000 permutations) were applied, and effect sizes were reported as permutation-derived rank-biserial correlations. Permutation *P*-values were Benjamini–Hochberg adjusted across comparisons. RNA-sequencing differential expression was performed with DESeq2, defining significance as adjusted $P < .05$ and $\log_2$ fold change ≥ 0.5. Gene set enrichment analysis (Reactome, Hallmark) and gene set variation analysis were used to assess pathway enrichment (false discovery rate < 0.05). Morphological profiling was analyzed through random forest classifiers and Uniform Manifold Approximation and Projection after feature filtering. All experiments were conducted in $\geq$3 biological replicates. Significance threshold was defined as adjusted $P < .05$.

ETHICS STATEMENT

The study was conducted in accordance with the Declaration of Helsinki and approved by the Institutional Medical Ethics Committee, SGS Life Science Services, Germany (protocol title: "Scientific analysis of surgical skin – Actinic Keratosis"; approval identification: IRB Ref. number 2020/124; SGS project number 201-01-1971/sponsor project number STDY-70005). Written informed consent was obtained from all donors prior to tissue collection. Facial skin explants from healthy individuals undergoing esthetic surgery were provided by Alphenyx (Marseille, France), which obtained all necessary authorizations from the French Ministry of Research and approval from the French Ethical Committee.

DATA AVAILABILITY STATEMENT

The datasets generated and analyzed during this study are available from the corresponding author upon reasonable request. RNA-sequencing data have been deposited as GSE305980 (https://www.ncbi.nlm.nih.gov/geo/query/acc.cgi?acc=GSE305980).

ORCIDs

Leonardo Elsbroek: http://orcid.org/0000-0003-0813-7047
Frank Lyko: http://orcid.org/0000-0002-4873-5431
Ludger Kolbe: http://orcid.org/0000-0001-8608-8901

CONFLICT OF INTEREST

LE, LK, AG, KR, PW, and MW are employees of Beiersdorf AG. FL and VS received consultation fees from Beiersdorf AG. The remaining authors state no conflict of interest.

ACKNOWLEDGMENTS

This work was funded by Beiersdorf AG. Actinic keratosis sample acquisition and patient recruitment were carried out by Dermatologikum Hamburg GmbH.

AUTHOR CONTRIBUTIONS

Conceptualization: LE, LK, KR, AG; Formal Analysis: LE; Funding Acquisition: MW; Methodology: LE; Resources: SK, VS, PW; Software: LE, PW; Supervision: FL, LK; Visualization: LE; Writing – Original Draft Preparation: LE; Writing – Review and Editing: LE, LK

SUPPLEMENTARY MATERIAL

Supplementary material is linked to the online version of the paper at www.jidonline.org, and at 10.1016/j.jid.2025.11.018.

REFERENCES

Almine JF, O'Hare CAJ, Dunphy G, Haga IR, Naik RJ, Atrih A, et al. IFI16 and cGAS cooperate in the activation of STING during DNA sensing in human keratinocytes. Nat Commun 2017;8:14392.

Bahamondes Lorca VA, Wu S. Ultraviolet light, unfolded protein response and autophagy(dagger). Photochem Photobiol 2023;99:498–508.

Bencomo T, Lee CS. Gene expression landscape of cutaneous squamous cell carcinoma progression. Br J Dermatol 2024;191:760–74.

Bluth MJ, Zaba LC, Moussai D, Suárez-Fariñas M, Kaporis H, Fan L, et al. Myeloid dendritic cells from human cutaneous squamous cell carcinoma are poor stimulators of T-cell proliferation. J Invest Dermatol 2009;129:2451–62.

Brash DE, Rudolph JA, Simon JA, Lin A, McKenna GJ, Baden HP, et al. A role for sunlight in skin cancer: UV-induced p53 mutations in squamous cell carcinoma. Proc Natl Acad Sci U S A 1991;88:10124–8.

Bray MA, Singh S, Han H, Davis CT, Borgeson B, Hartland C, et al. Cell Painting, a high-content image-based assay for morphological profiling using multiplexed fluorescent dyes. Nat Protoc 2016;11:1757–74.

Chen K, Liu J, Cao X. cGAS-STING pathway in senescence-related inflammation. Natl Sci Rev 2018;5:308–10.

Chitsazzadeh V, Coarfa C, Drummond JA, Nguyen T, Joseph A, Chilukuri S, et al. Cross-species identification of genomic drivers of squamous cell carcinoma development across preneoplastic intermediates. Nat Commun 2016;7:12601.

Dalmau N, Andrieu-Abadie N, Tauler R, Bedia C. Phenotypic and lipidomic characterization of primary human epidermal keratinocytes exposed to simulated solar UV radiation. J Dermatol Sci 2018;92:97–105.

de Pedro I, Alonso-Lecue P, Sanz-Gómez N, Freije A, Gandarillas A. Sublethal UV irradiation induces squamous differentiation via a p53-independent, DNA damage-mitosis checkpoint. Cell Death Dis 2018;9:1094.

DiGiovanna JJ, Kraemer KH. Shining a light on xeroderma pigmentosum. J Invest Dermatol 2012;132:785–96.

Dorr MM, Rochette PJ. Reduction of DNA damage repair efficiency and accumulation of residual damage following chronic UVB-irradiation of HaCaT cells. PLOS One 2023;18:e0283572.

Dunn J, Potter M, Rees A, Rünger TM. Activation of the fanconi anemia/BRCA pathway and recombination repair in the cellular response to solar ultraviolet light. Cancer Res 2006;66:11140–7.

Dunphy G, Flannery SM, Almine JF, Connolly DJ, Paulus C, Jønsson KL, et al. Non-canonical activation of the DNA sensing adaptor STING by ATM and IFI16 mediates NF-κB signaling after nuclear DNA damage. Mol Cell 2018;71:745–60.e5.

Edwards L, Berman B, Rapini RP, Whiting DA, Tyring S, Greenway HT, et al. Treatment of cutaneous squamous cell carcinomas by intralesional interferon alfa-2b therapy. Arch Dermatol 1992;128:1486–9.

Ewald J, Zhou G, Lu Y, Xia J. Using ExpressAnalyst for comprehensive gene expression analysis in model and non-model organisms. Curr Protoc 2023;3:e922.

Feldmeyer L, Keller M, Niklaus G, Hohl D, Werner S, Beer HD. The inflammasome mediates UVB-induced activation and secretion of interleukin-1beta by keratinocytes. Curr Biol 2007;17:1140–5.

Garcia-Diaz A, Shin DS, Moreno BH, Saco J, Escuin-Ordinas H, Rodriguez GA, et al. Interferon receptor signaling pathways regulating PD-L1 and PD-L2 expression. Cell Rep 2017;19:1189–201.

Gregorio J, Meller S, Conrad C, Di Nardo A, Homey B, Lauerma A, et al. Plasmacytoid dendritic cells sense skin injury and promote wound healing through type I interferons. J Exp Med 2010;207:2921–30.

Hänzelmann S, Castelo R, Guinney J. GSVA: gene set variation analysis for microarray and RNA-seq data. BMC Bioinform 2013;14:7.

He J, Guo Y, Chen J, Xu J, Zhu X. Exploring the correlation between UVB sensitivity and SLE activity: insights into UVB-driven pathogenesis in lupus erythematosus. J Autoimmun 2025;153:103393.

Iannacone MR, Sinnya S, Pandeya N, Isbel N, Campbell S, Fawcett J, et al. Prevalence of skin cancer and related skin tumors in high-risk kidney and liver transplant recipients in Queensland, Australia. J Invest Dermatol 2016;136:1382–6.

Jassal B, Matthews L, Viteri G, Gong C, Lorente P, Fabregat A, et al. The reactome pathway knowledgebase. Nucleic Acids Res 2020;48:D498–503.

Joly F, Deret S, Gamboa B, Menigot C, Fogel P, Mounier C, et al. Photodynamic therapy corrects abnormal cancer-associated gene expression observed in actinic keratosis lesions and induces a remodeling effect in photodamaged skin. J Dermatol Sci 2018. S0923-1811(17)30775-2.

Kamada R, Yang W, Zhang Y, Patel MC, Yang Y, Ouda R, et al. Interferon stimulation creates chromatin marks and establishes transcriptional memory. Proc Natl Acad Sci U S A 2018;115:E9162–71.

Kang JA, Kim YJ, Jeon YJ. The diverse repertoire of ISG15: more intricate than initially thought. Exp Mol Med 2022;54:1779–92.

Kim YS, Shin S, Jung SH, Park YM, Park GS, Lee SH, et al. Genomic progression of precancerous actinic keratosis to squamous cell carcinoma. J Invest Dermatol 2022;142:528–38.e8.

Kondo S, Aso K. Establishment of a cell line of human skin squamous cell carcinoma in vitro. Br J Dermatol 1981;105:125–32.

Korsunsky I, Millard N, Fan J, Slowikowski K, Zhang F, Wei K, et al. Fast, sensitive and accurate integration of single-cell data with Harmony. Nat Methods 2019;16:1289–96.

Kumagai Y, Nio-Kobayashi J, Ishihara S, Enomoto A, Akiyama M, Ichihara R, et al. The interferon-β/STAT1 axis drives the collective invasion of skin squamous cell carcinoma with sealed intercellular spaces. Oncogenesis 2022;11:27.

Lacarrubba F, Nasca MR, Micali G. Advances in the use of topical imiquimod to treat dermatologic disorders. Ther Clin Risk Manag 2008;4:87–97.

Landrum MJ, Chitipiralla S, Brown GR, Chen C, Gu B, Hart J, et al. ClinVar: improvements to accessing data. Nucleic Acids Res 2020;48:D835–44.

Lawrence M, Huber W, Pagès H, Aboyoun P, Carlson M, Gentleman R, et al. Software for computing and annotating genomic ranges. PLOS Comput Biol 2013;9:e1003118.

Lee DH, Pfeifer GP. Deamination of 5-methylcytosines within cyclobutane pyrimidine dimers is an important component of UVB mutagenesis. J Biol Chem 2003;278:10314–21.

Li C, Liu W, Wang F, Hayashi T, Mizuno K, Hattori S, et al. DNA damage-triggered activation of cGAS-STING pathway induces apoptosis in human keratinocyte HaCaT cells. Mol Immunol 2021;131:180–90.

Li T, Chen ZJ. The cGAS-cGAMP-STING pathway connects DNA damage to inflammation, senescence, and cancer. J Exp Med 2018;215:1287–99.

Li YY, Hanna GJ, Laga AC, Haddad RI, Lorch JH, Hammerman PS. Genomic analysis of metastatic cutaneous squamous cell carcinoma. Clin Cancer Res 2015;21:1447–56.

Liberzon A, Birger C, Thorvaldsdóttir H, Ghandi M, Mesirov JP, Tamayo P. The Molecular Signatures Database (MSigDB) hallmark gene set collection. Cell Syst 2015;1:417–25.

Lin Y, Cao Z, Lyu T, Kong T, Zhang Q, Wu K, et al. Single-cell RNA-seq of UVB-radiated skin reveals landscape of photoaging-related inflammation and protection by vitamin D. Gene 2022;831:146563.

Loftus SN, Gharaee-Kermani M, Xu B, Moore TM, Hannoudi A, Mallbris MJ, et al. Interferon alpha promotes caspase-8 dependent ultraviolet light-mediated keratinocyte apoptosis via interferon regulatory factor 1. Front Immunol 2024;15:1384606.

Love MI, Huber W, Anders S. Moderated estimation of fold change and dispersion for RNA-seq data with DESeq2. Genome Biol 2014;15:550.

Mann T, Eggers K, Rippke F, Tesch M, Buerger A, Darvin ME, et al. High-energy visible light at ambient doses and intensities induces oxidative stress of skin-Protective effects of the antioxidant and Nrf2 inducer Licochalcone A in vitro and in vivo. Photodermatol Photoimmunol Photomed 2020;36:135–44.

Martincorena I, Roshan A, Gerstung M, Ellis P, Van Loo P, McLaren S, et al. Tumor evolution. High burden and pervasive positive selection of somatic mutations in normal human skin. Science 2015;348:880–6.

Mitsui H, Suárez-Fariñas M, Gulati N, Shah KR, Cannizzaro MV, Coats I, et al. Gene expression profiling of the leading edge of cutaneous squamous cell carcinoma: il-24-driven MMP-7. J Invest Dermatol 2014;134:1418–27.

Nindl I, Dang C, Forschner T, Kuban RJ, Meyer T, Sterry W, et al. Identification of differentially expressed genes in cutaneous squamous cell carcinoma by microarray expression profiling. Mol Cancer 2006;5:30.

Obenchain V, Lawrence M, Carey V, Gogarten S, Shannon P, Morgan M. VariantAnnotation: a Bioconductor package for exploration and annotation of genetic variants. Bioinformatics 2014;30:2076–8.

Ooi T, Barnetson RS, Zhuang L, McKane S, Lee JH, Slade HB, et al. Imiquimod-induced regression of actinic keratosis is associated with infiltration by T lymphocytes and dendritic cells: a randomized controlled trial. Br J Dermatol 2006;154:72–8.

Park JM, Yang SW, Yu KR, Ka SH, Lee SW, Seol JH, et al. Modification of PCNA by ISG15 plays a crucial role in termination of error-prone translesion DNA synthesis. Mol Cell 2014;54:626–38.

Qiu J, Xu B, Ye D, Ren D, Wang S, Benci JL, et al. Cancer cells resistant to immune checkpoint blockade acquire interferon-associated epigenetic memory to sustain T cell dysfunction. Nat Cancer 2023;4:43–61.

Raso MC, Djoric N, Walser F, Hess S, Schmid FM, Burger S, et al. Interferon-stimulated gene 15 accelerates replication fork progression inducing chromosomal breakage. J Cell Biol 2020;219:e202002175.

Rodríguez-Paredes M, Bormann F, Raddatz G, Gutekunst J, Lucena-Porcel C, Köhler F, et al. Methylation profiling identifies two subclasses of squamous cell carcinoma related to distinct cells of origin. Nat Commun 2018;9:577.

Sandy Z, da Costa IC, Schmidt CK. More than meets the ISG15: emerging roles in the DNA damage response and beyond. Biomolecules 2020;10:1557.

Schneider VA, Graves-Lindsay T, Howe K, Bouk N, Chen HC, Kitts PA, et al. Evaluation of GRCh38 and de novo haploid genome assemblies demonstrates the enduring quality of the reference assembly. Genome Res 2017;27:849–64.

Shime H, Odanaka M, Imai M, Sugiyama D, Takayama S, Morita A, et al. UVB irradiation expands skin-resident CD81+Foxp3+ regulatory T cells with a highly activated phenotype. J Invest Dermatol 2025;145:1770–80.e11.

Sinha S, Ng V, Novaj A, Zhu Y, Yazaki S, Pei X, et al. The cold immunological landscape of ATM-deficient cancers. J Immunother Cancer 2025;13:e010548.

Skopelja-Gardner S, An J, Tai J, Tanaka L, Sun X, Hermanson P, et al. The early local and systemic Type I interferon responses to ultraviolet B light exposure are cGAS dependent. Sci Rep 2020;10:7908.

Solé-Boldo L, Raddatz G, Gutekunst J, Gilliam O, Bormann F, Liberio MS, et al. Differentiation-related epigenomic changes define clinically distinct keratinocyte cancer subclasses. Mol Syst Biol 2022;18:e11073.

Stirling DR, Swain-Bowden MJ, Lucas AM, Carpenter AE, Cimini BA, Goodman A. CellProfiler 4: improvements in speed, utility and usability. BMC Bioinform 2021;22:433.

Stuart T, Butler A, Hoffman P, Hafemeister C, Papalexi E, Mauck WM 3rd, et al. Comprehensive integration of single-cell data. Cell 2019;177:1888–902.e21.

Subramanian A, Tamayo P, Mootha VK, Mukherjee S, Ebert BL, Gillette MA, et al. Gene set enrichment analysis: a knowledge-based approach for interpreting genome-wide expression profiles. Proc Natl Acad Sci U S A 2005;102:15545–50.

Tandukar B, Deivendran D, Chen L, Cruz-Pacheco N, Sharma H, Xu A, et al. Genetic evolution of keratinocytes to cutaneous squamous cell carcinoma. bioRxiv 2024;2024.07.23:604673.

Thomson J, Bewicke-Copley F, Anene CA, Gulati A, Nagano A, Purdie K, et al. The genomic landscape of actinic keratosis. J Invest Dermatol 2021;141:1664–74.e7.

Torres A, Storey L, Anders M, Miller RL, Bulbulian BJ, Jin J, et al. Immune-mediated changes in actinic keratosis following topical treatment with imiquimod 5% cream. J Transl Med 2007;5:7.

Traianou A, Ulrich M, Apalla Z, De Vries E, Bakirtzi K, Kalabalikis D, et al. Risk factors for actinic keratosis in eight European centres: a case-control study. Br J Dermatol 2012;167(Suppl. 2):36–42.

Ueyama A, Yamamoto M, Tsujii K, Furue Y, Imura C, Shichijo M, et al. Mechanism of pathogenesis of imiquimod-induced skin inflammation in the mouse: a role for interferon-alpha in dendritic cell activation by imiquimod. J Dermatol 2014;41:135–43.

Weichselbaum RR, Ishwaran H, Yoon T, Nuyten DSA, Baker SW, Khodarev N, et al. An interferon-related gene signature for DNA damage resistance is a predictive marker for chemotherapy and radiation for breast cancer. Proc Natl Acad Sci U S A 2008;105:18490–5.

Wenzel J, Tomiuk S, Zahn S, Küsters D, Vahsen A, Wiechert A, et al. Transcriptional profiling identifies an interferon-associated host immune response in invasive squamous cell carcinoma of the skin. Int J Cancer 2008;123:2605–15.

Winge MCG, Kellman LN, Guo K, Tang JY, Swetter SM, Aasi SZ, et al. Advances in cutaneous squamous cell carcinoma. Nat Rev Cancer 2023;23:430–49.

Wright MN, Ziegler A. ranger: A Fast Implementation of Random Forests for High Dimensional Data in C++ and R. Journal of Statistical Software 2017;77.

Wu R, Yang H, Liu C. IFIT3: a crucial mediator in innate immunity and tumor progression with therapeutic implications. Front Immunol 2025;16:1515718.

Xiang F, Lucas R, Hales S, Neale R. Incidence of nonmelanoma skin cancer in relation to ambient UV radiation in white populations, 1978–2012: empirical relationships. JAMA Dermatol 2014;150:1063–71.

Yang H, Wang H, Ren J, Chen Q, Chen ZJ. cGAS is essential for cellular senescence. Proc Natl Acad Sci U S A 2017;114:E4612–20.

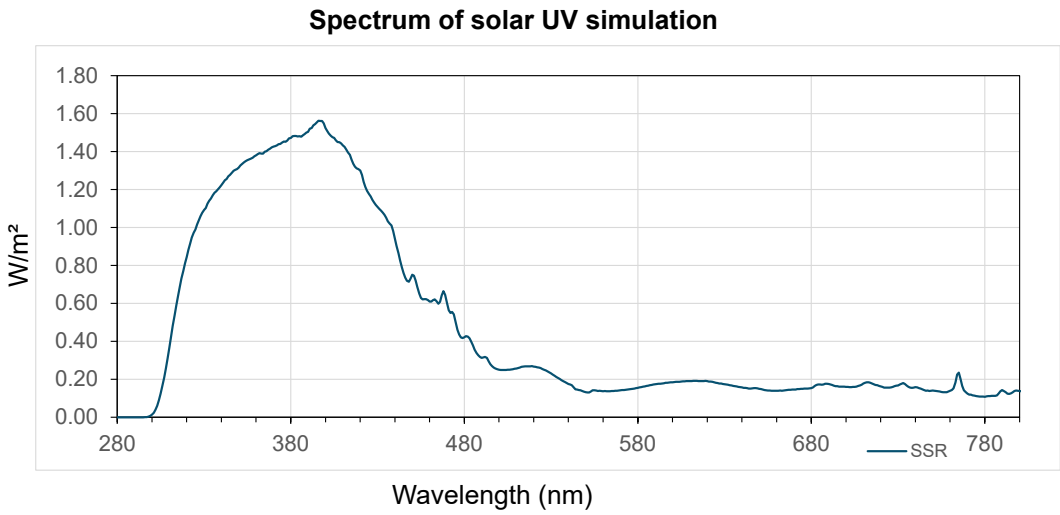
Young AR, Orchard GE, Harrison GI, Klock JL. The detrimental effects of daily sub-erythemal exposure on human skin in vivo can be prevented by a daily-care broad-spectrum sunscreen. J Invest Dermatol 2007;127:975–8.

Yu R, Zhu B, Chen D. Type I interferon-mediated tumor immunity and its role in immunotherapy. Cell Mol Life Sci 2022;79:191.

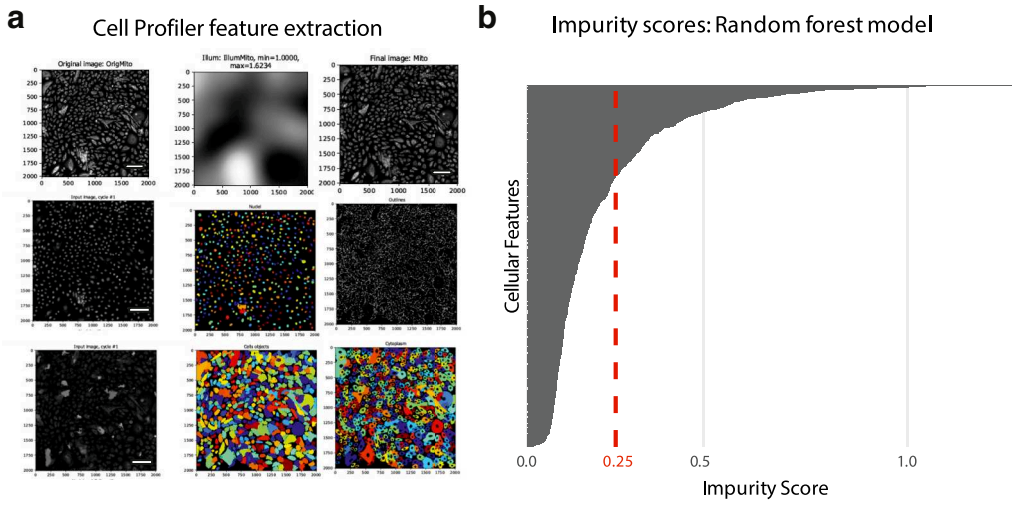
Yuan X, Li H, Lee JS, Lee DH. Role of mitochondrial dysfunction in UV-induced photoaging and skin cancers. Exp Dermatol 2025;34:e70114.

Zeng Z, Veitch M, Kelly GA, Tuong ZK, Cruz JG, Frazer IH, et al. IFN-γ critically enables the intratumoural infiltration of CXCR3+ CD8+ T cells to drive squamous cell carcinoma regression. Cancers (Basel) 2021;13:2131.

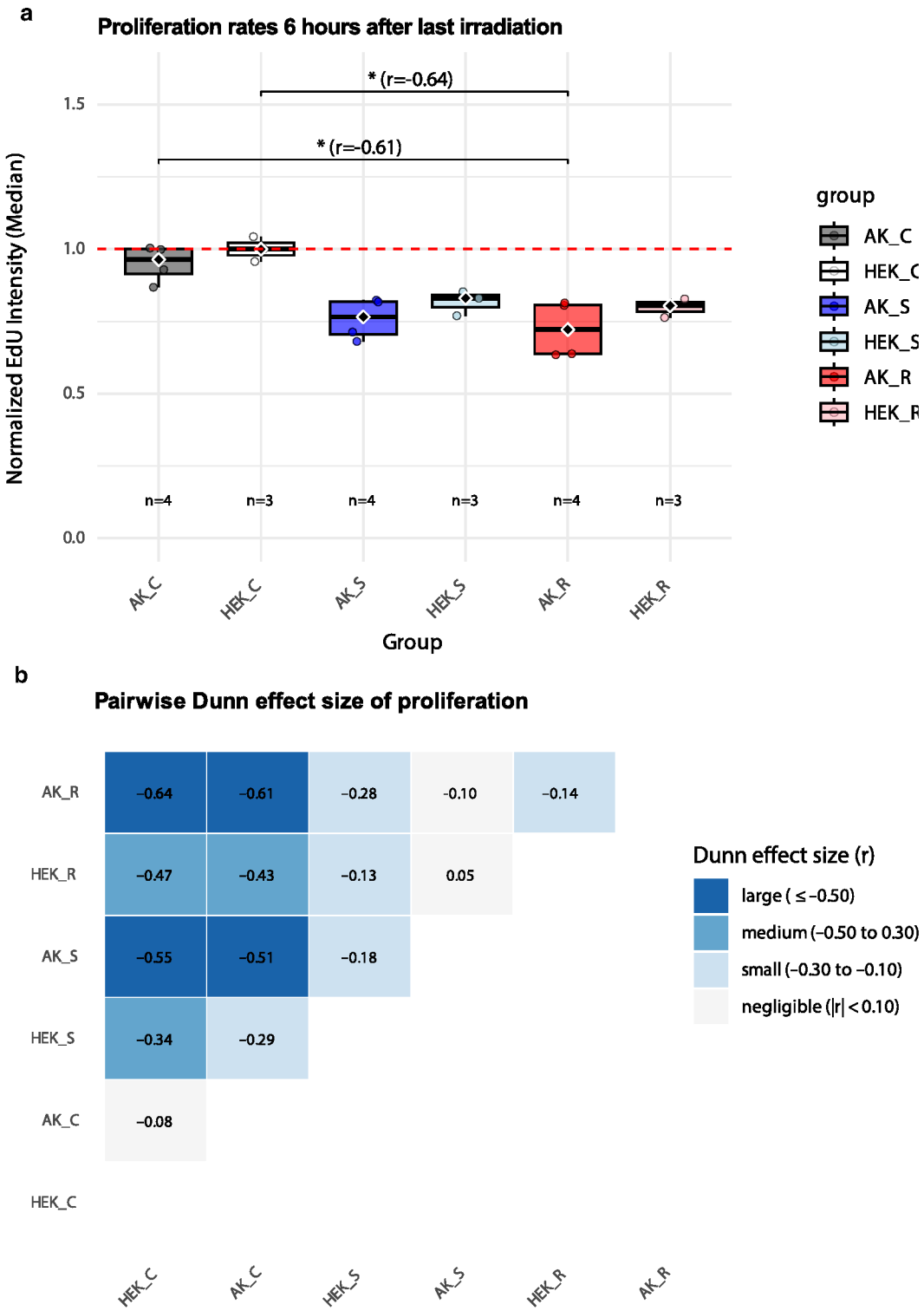
Zou DD, Sun YZ, Li XJ, Wu WJ, Xu D, He YT, et al. Single-cell sequencing highlights heterogeneity and malignant progression in actinic keratosis and cutaneous squamous cell carcinoma. eLife 2023;12:e85270.



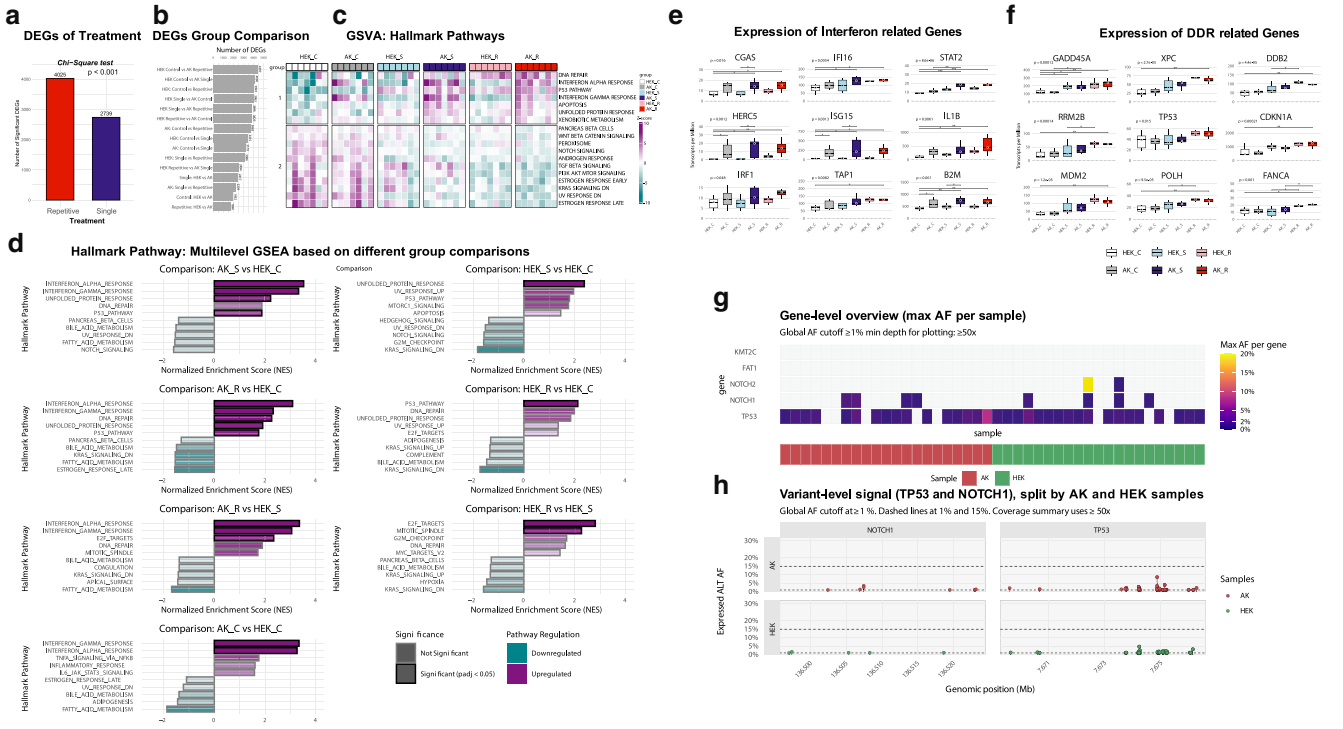
Supplementary Figure S1. Spectral characteristics of the Oriel SSR used for UV irradiation. Shown is a spectral energy distribution (W/m^2) of the Oriel solar simulator equipped with a dichroic mirror reflecting in the UV range (280–400 nm) and a N-WG320 cutoff filter (Schott, Germany), measured across 280–800 nm. SSR, solar UV simulator radiation.



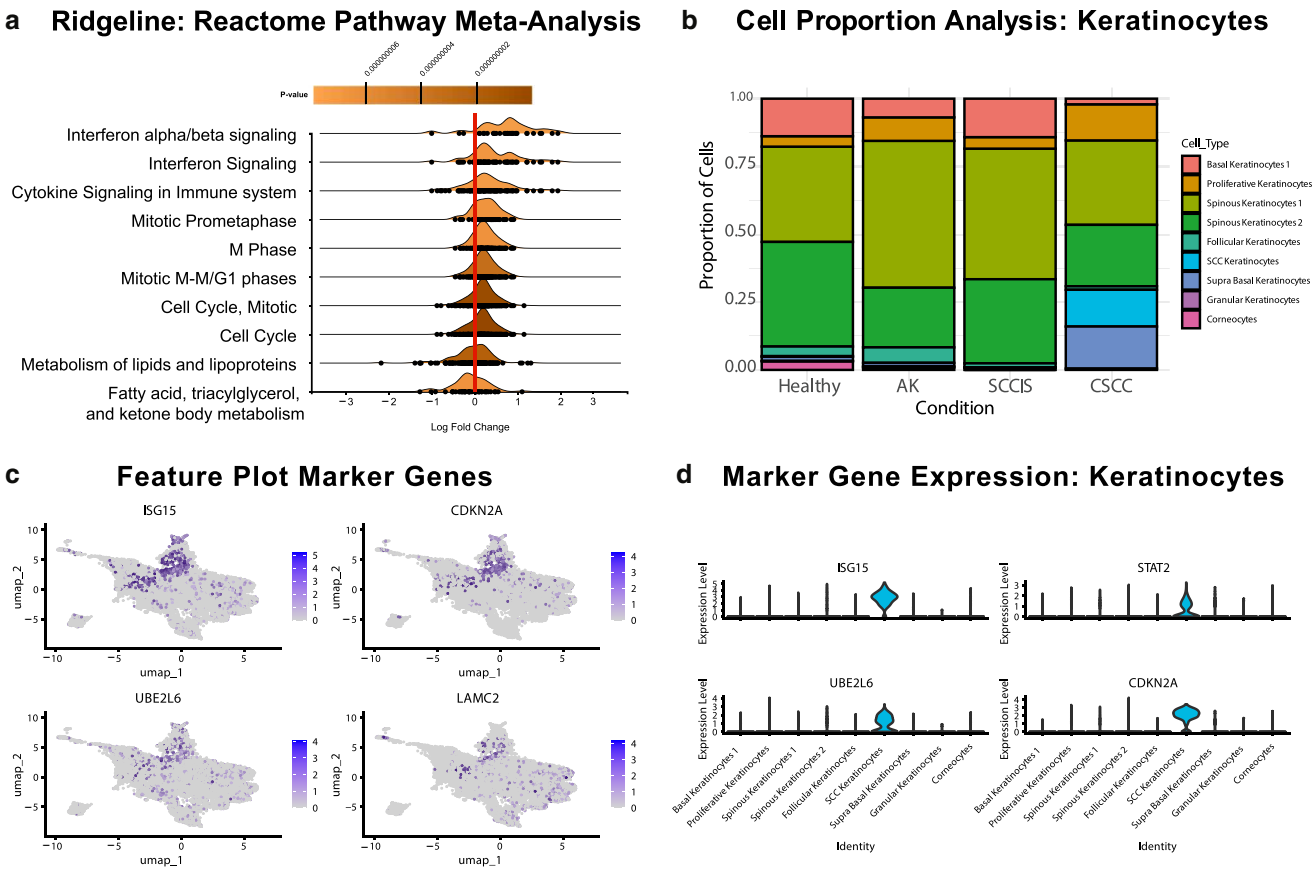
Supplementary Figure S2. Extended morphological feature analysis of irradiated keratinocytes. (**a**) CellProfiler segmentation was used for cell and cytoplasm identification. Masks were applied across fluorescent channels to extract cellular features. Axes indicate pixel coordinates. Bar = 100 μm. (**b**) Feature importance ranking based on impurity scores from a random forest classifier. Features with scores >0.25 were retained for downstream dimensionality reduction and clustering.



Supplementary Figure S3. Proliferation rates after single and repetitive irradiation. (**a**) Median-normalized EdU intensity 6 hours after irradiation. EdU levels were normalized to unirradiated HEK controls; the red dashed line denotes baseline. Statistical significance was first evaluated using the Kruskal–Wallis test, followed by Dunn's posthoc test for pairwise group comparisons; significant comparisons are shown with asterisk. (T6: HEK: n = 3 donors, AK: n = 4 donors). Color coding: HEK control (white), single UV (light blue), repeated UV (light red), AK control (dark gray), single UV (dark blue), and repeated UV (dark red). (**b**) Heatmap of pairwise effect sizes from Dunn's posthoc test of EdU after 6 hours. The color scale represents the magnitude and direction of the effect size, binned as small ($r > -0.3$), medium ($-0.5 < r \leq -0.3$), and large ($r \leq -0.5$). AK, actinic keratosis; EdU, 5-ethynyl-2′-deoxyuridine; HEK, healthy epidermal keratinocyte.



Supplementary Figure S4. Extended transcriptomic analysis of UV responses in AK keratinocytes. (**a**) Total DEGs after single (blue) or repetitive (red) UV in AK keratinocytes. (**b**) Pairwise DEG counts across experimental groups. (**c**) GSVA heatmap of Hallmark pathways (adjusted $P < .05$). Z-scored enrichment values are shown; group coloring is consistent with that in Figure 4. (**d**) Summary plot of significantly enriched pathways (adjusted $P < .05$). Color denotes up/downregulation. (**e**) TPM boxplots of selected IFN genes. Statistical analysis was by Kruskal–Wallis with Dunn's posthoc test. (**f**) TPM boxplots of selected DDR genes. Statistical analysis was by Kruskal–Wallis with Dunn's posthoc test. (**g**) RNA-sequencing–based variant screening of frequently mutated genes in AK/cSCC. Maximum expressed alternative AF per sample after QC filtering (≥50× coverage, ≥5 ALT-supporting reads, AF ≥ 1%, q < 0.001). Each point represents the highest detected pathogenic SNV from ClinVar for AK and HEK samples. (**h**) Lollipop plots showing the distribution and expressed AF of detected ClinVar-annotated variants in TP53 and NOTCH1. Each dot indicates a site-specific variant observed across samples, with AF scaled to the expressed variant frequency. AF, allele frequency; AK, actinic keratosis; cSCC, cutaneous squamous cell carcinoma; DDR, DNA damage response; DEG, differentially expressed gene; GSVA, gene set variation analysis; HEK, healthy epidermal keratinocyte; QC, quality control; SNV, single-nucleotide variant; TPM, transcript per million.



Supplementary Figure S5. Expanded pathway and marker gene analysis in AK and SCC keratinocytes. (**a**) Ridgeline plot showing Reactome pathway enrichment (log_2 fold change) comparing AK lesions with control skin across independent datasets. Each ridge represents the distribution of pathway activation scores, with significantly enriched pathways scaled in amplitude. The red vertical line indicates the baseline (log_2 fold change = 0). (**b**) Cell proportion analysis of keratinocyte subpopulations in Zou et al (2023). Arising SCC cluster is highlighted in dark gray. (**c**) Feature plots showing expression of marker genes in SCC-associated keratinocytes. (**d**) Marker gene expression across keratinocyte subpopulations. AK, actinic keratosis; SCC, squamous cell carcinoma.